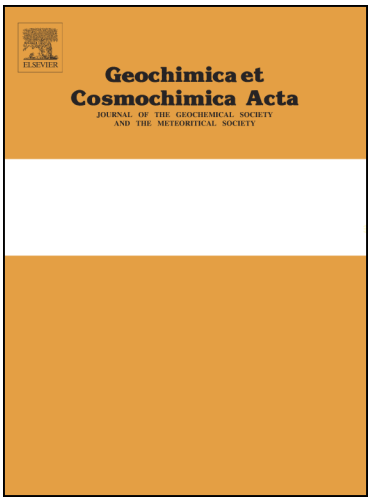

The Dissolution Behavior of Borosilicate Glasses in Far-From Equilibrium Conditions

James J. Neeway, Peter C. Rieke, Benjamin P. Parruzot, Joseph V. Ryan, R. Matthew Asmussen

PII: S0016-7037(18)30070-X
DOI: https://doi.org/10.1016/j.gca.2018.02.001
Reference: GCA 10643

To appear in: *Geochimica et Cosmochimica Acta*

Received Date: 10 June 2017
Accepted Date: 1 February 2018

Please cite this article as: Neeway, J.J., Rieke, P.C., Parruzot, B.P., Ryan, J.V., Matthew Asmussen, R., The Dissolution Behavior of Borosilicate Glasses in Far-From Equilibrium Conditions, *Geochimica et Cosmochimica Acta* (2018), doi: https://doi.org/10.1016/j.gca.2018.02.001

The Dissolution Behavior of Borosilicate Glasses in Far-From Equilibrium Conditions

Authors:

James J. Neeway [a,*], Peter C. Rieke [a], Benjamin P. Parruzot [a], Joseph V. Ryan [a], R. Matthew Asmussen [a]

Affiliation:

[a] *Energy and Environment Directorate, Pacific Northwest National Laboratory, Richland, WA 99352, USA*

*** Corresponding Author:**

+1 509-375-5397

James.Neeway@pnnl.gov

ABSTRACT

An area of agreement in the waste glass corrosion community is that, at far-from-equilibrium conditions, the dissolution of borosilicate glasses used to immobilize nuclear waste is known to be a function of both temperature and pH. The aim of this work is to study the effects of temperature and pH on the dissolution rate of three model nuclear waste glasses (SON68, ISG, AFCI). The dissolution rate data are then used to parameterize a kinetic rate model based on Transition State Theory that has been developed to model glass corrosion behavior in dilute conditions. To do this, experiments were conducted at temperatures of 23, 40, 70, and 90 °C and pH(22 °C) values of 9, 10, 11, and 12 with the single-pass flow-through (SPFT) test method. Both the absolute dissolution rates and the rate model parameters are compared with previous results. Rate model parameters for the three glasses studied here are nearly equivalent within error and in relative agreement with previous studies though quantifiable differences exist. The glass dissolution rates were analyzed with a linear multivariate regression (LMR) and a nonlinear multivariate regression performed with the use of the Glass Corrosion Modeling Tool (GCMT), with which a robust uncertainty analysis is performed. This robust analysis highlights the high degree of correlation of various parameters in the kinetic rate model. As more data are obtained on borosilicate glasses with varying compositions, a mathematical description of the effect of glass composition on the rate parameter values should be possible. This would allow for the possibility of calculating the forward dissolution rate of glass based solely on composition. In addition, the method of determination of parameter uncertainty and correlation provides a framework for other rate models that describe the dissolution rates of other amorphous and crystalline materials in a wide range of chemical conditions. The higher level of uncertainty analysis would provide a basis for comparison of different rate models and allow for a better means of quantifiably comparing the various models.

1. INTRODUCTION

Upon contact with water, glass corrodes and constituents of the glass are released into solution. This glass-water reaction, principally of borosilicate glass, is of interest in the field of nuclear waste management. Specifically, glass is a material in which nuclear waste is immobilized and the release of radionuclides into the environment upon waste glass disposal will be controlled by the dissolution rate of the glass matrix (Birkholzer et al. 2012). Because of the importance of the glass-water reaction in controlling the release of radionuclides into the environment, six nations (USA, Japan, France, Belgium, UK, and Germany) are participating in an international initiative to understand the long-term behavior of high-level nuclear waste glasses (Gin et al. 2013).

One of the primary goals of the international nuclear waste glass corrosion community is to develop mechanistic performance assessment models that can be used to demonstrate the feasibility of glass disposal in various geological environments (Gin et al. 2013). The dissolution rate of borosilicate glasses depends on several factors including glass composition, temperature, pH, and the chemical composition of the aqueous solution. For convenience, the corrosion rate of glass in static conditions has been divided into three stages of dissolution plus a "transition" between the first and second stage. In the first stage, there is a relatively fast release of components into solution. As the reaction proceeds and dissolved species build in solution, an alteration layer containing less soluble species (Al, Si, Zr) forms between the pristine glass and solution. The transition from dilute to saturated conditions is concurrent with the formation of an alteration layer and a slowing of the glass dissolution rate. The second and third stages of glass dissolution involve a slow residual rate of glass dissolution (Frugier et al. 2008, Gin et al. 2011, Grambow 1985, McGrail et al. 2001a) and a delayed acceleration in the dissolution rate (Fournier et al. 2014, Strachan and Croak 2000, Strachan and Neeway 2014, Van Iseghem and Grambow 1988), respectively. The focus of this paper is on the first stage of glass dissolution and, to a lesser extent, the transition to the second stage.

Possible processes responsible for controlling the breakdown of the glass network include matrix dissolution, ion exchange/interdiffusion, water diffusion, passivation layer formation, and secondary phase precipitation and growth. The combination of processes that control the glass dissolution rate, especially as the contacting solution transitions from dilute to saturated conditions with respect to the formation of secondary phases, is a subject of debate (Geisler et al. 2015, Gin et al. 2015, Gin et al. 2016). However, at short time periods when the solution is relatively dilute and the alteration layer does not affect glass dissolution, it is generally agreed upon that a

combination of ion exchange and matrix dissolution control the glass dissolution rate (Gin et al. 2013, Van Iseghem et al. 2009). When a Transition State Theory (TST) rate equation is used to model the glass dissolution rate in unsaturated conditions, the rate model parameters are known to vary but, until now, a concerted effort to understand the significance of varying rate law parameters has not been undertaken.

In this paper, we present experimental results of the dissolution rates for three simulant waste glass compositions that were chosen for reasons described in Section 1.3. The study of these glasses expands the available data on nuclear waste glass dissolution. The dissolution rates are used to determine rate model parameters and parameter uncertainties for dissolution rate models that are being envisioned for implementation in predicting the corrosion behavior of nuclear waste glasses in geological repositories. The rate model parameters obtained for the three glasses presented here are compared to literature values of a wide range of other waste glass compositions. We discuss how the modeling effort performed in this study 1) can be used to compare the relative difference in rate model parameters of different glasses and 2) provide a basis for confining a rate model parameter confidence space for different glasses. The modeling and uncertainty approach may be useful for other rate models that describe the dissolution rates of other amorphous and crystalline materials in a wide range of chemical conditions (Gudbrandsson et al. 2014, Pollyea and Rimstidt 2017, Schaef and McGrail 2009).

1.1 Glass Dissolution Rate Model

The rate of the dissolution of the silicate network can be described through TST, which describes the rate at which the activated complex (a transitional aggregate of atoms that form during the collision process) changes from reactants to products, and which limits the rate at which the overall reaction can proceed (Eyring 1935). Åagaard and Helgeson (1982) provided a general rate equation for the rate of mineral decomposition based on TST. Grambow (1985) argued that the rate-limiting reaction that best describes glass dissolution is the dissolution of SiO_2 to form silicic acid:

$$SiO_{2(s)} + 2H_2O \leftrightarrow SiO_2 \cdot 2H_2O^{\ddagger} \rightarrow H_4SiO_{4(aq)} \qquad \text{Eq. 1}$$

where $SiO_2 \bullet 2H_2O^{\ddagger}$ represents an activated complex. However, when discussing models that describe glass corrosion, it must be noted that glass-water interaction involves many coupled and simultaneous reactions and a single model that addresses all of these behaviors has not yet been developed. In Eq. 1, the double-headed arrow

links the reactants and the activated complex, symbolizing a reversible reaction. In contrast, the decomposition to, and subsequent migration of, $H_4SiO_{4(aq)}$ is an irreversible reaction (Pederson et al. 1986). Assuming Eq. 1 is the rate limiting reaction, the TST model can then written as:

$$r_i = \nu_i k_0 a_{H^+}^{-\eta} \exp\left(\frac{-E_a}{RT}\right)\left[1-\left(\frac{Q}{K_g}\right)^{1/\sigma}\right] \quad \text{Eq. 2}$$

where r_i is the glass dissolution rate based on element i (g m^{-2} d^{-1}), k_0 is the intrinsic rate constant (g m^{-2} d^{-1}), ν_i is the stoichiometric coefficient of element i in the glass (unitless), a_{H+} is the hydrogen ion activity, η is the pH power law coefficient, E_a is the apparent activation energy (J mol^{-1}), R is the ideal gas constant, T is the absolute temperature, Q is the ion activity product, K_g is defined as the pseudo-equilibrium constant, and σ is the Temkin coefficient. It has been argued that σ is equal to one because any value where σ is not equal to one is inconsistent with TST (Lasaga 1995). We also note that Eq. 2 is only applicable in the alkaline range, specifically where the log of the glass dissolution rate shows a linear dependence with changes in pH. This is discussed further in Section 4.4.

In systems where the concentration of H_4SiO_4 is low, the affinity portion of Eq. 2 can be ignored and rewritten to account for the rate of release of any element i released from the glass into the aqueous phase as a function of pH and temperature:

$$r_i = \nu_i k_0 a_{H^+}^{-\eta} \exp\left(\frac{-E_a}{RT}\right) \quad \text{Eq. 3}$$

Eq. 3 provides the overall rate for all reactions contributing to glass dissolution. Through the ν_i term, the glass dissolution rate can be indexed to a wide range of elements present in the glass. In the absence of an affinity effect, Eq. 3 represents the glass dissolution rate in dilute conditions and is often referred to as the forward dissolution rate. The overlying assumption, which is supported by experimental evidence, is that the release of elements from the glass is stoichiometric in forward rate conditions.

1.3 Experimental Aim

One aim of the set of experiments described in the present study is to measure the forward rate of glass dissolution with the single-pass flow-through (SPFT) method for three simulant high-level waste (HLW) glasses

(SON68, AFCI, and ISG) and to parameterize the model presented in Eq. 3. The glasses were chosen for various reasons: 1) as a link to a simulant glass composition to the R7T7 radioactive waste glass that is currently produced in France (SON68), 2) as a link to a current internal initiative on the long-term performance of waste glass where one glass composition is studied by several laboratories (ISG), and 3) to study the dissolution behavior of a glass that has been developed for the immobilization of radioactive waste from advanced nuclear fuel cycles (AFCI) (Crum et al. 2009).

The experimental data presented in the present study primarily focuses on data collected in dilute conditions where the glass dissolves at the forward rate. As the forward dissolution rate is generally understood to be controlled by surface reactions (Grambow 1985, Lasaga 1984), the present investigation examines glass alteration in dilute conditions and avoids the inherent complexities in the interpretation of rates when an alteration layer has formed at the glass surface (Bourcier et al. 1990, Geisler et al. 2015, Gin et al. 2015). The SPFT method, which precludes solution recycle, is common in the geochemistry community, where it has been employed to measure reaction rates of both minerals (Cantrell et al. 2013, Dove and Crerar 1990, Gudbrandsson et al. 2014, Hamilton et al. 2000, Oelkers et al. 2008) and glasses (Cassingham et al. 2015, Icenhower et al. 2008, Icenhower and Steefel 2013, Neeway et al. 2011, Pierce et al. 2010). To parameterize Eq. 3, rates were obtained in dilute conditions where the system is far from apparent equilibrium. Conducting the experiment at forward rate conditions allows for the effect of pH and temperature to be independently varied and quantified.

Parameters for the rate model presented in Eq. 3 were determined by performing a linear multivariate regression (LMR) and a nonlinear multivariate regression across all the dissolution rates determined at four test temperatures (22 °C, 40 °C, 70 °C, and 90 °C) and four pH values [pH(22 °C) 9, 10, 11, and 12]. The nonlinear multivariate regression was performed with the use of the Glass Corrosion Modeling Tool (GCMT) (Rieke and Kerisit 2016). Modeling with the GCMT method, which allows for a much more robust analysis of uncertainties in rate law parameters compared to the LMR method, has highlighted the high degree of correlation between rate law parameters, a topic that until now, has been largely overlooked. The rate parameters from the regression methods are provided for the three glasses tested here and compared with literature values for other borosilicate glasses.

2. EXPERIMENTAL PROCEDURE

2.1 Glass Fabrication and Preparation

The AFCI (Advanced Fuel Cycle Initiative) and SON68 glasses were fabricated at PNNL while the ISG (International Simple Glass) glass was supplied by MoSci (Rolla, MO, USA). The SON68 glass is the non-radioactive simulant of the radioactive R7T7 glass produced at the La Hague facility in France (Frugier et al. 2008). The ISG glass is part of a large batch that was fabricated to be used in an international effort to reach a consensus on the mechanisms controlling the long-term glass dissolution rate (Gin et al. 2013). The AFCI glass was developed as part of the U.S. Department of Energy (DOE) Advanced Fuel Cycle Initiative as a reference borosilicate glass for the immobilization of waste streams from the recycling of used nuclear fuel (Crum et al. 2009). The molar ratios of Si/B, Si/Na, and Si/Al for both ISG and SON68 are the same and equal to 1.88, 2.40, and 7.87, respectively. The compositions of the major oxides in the three glasses in mass% and mol% are presented in Table 1.

Table 1. List of glass compositions in mass%, mol%, normalization factor for Si, Na, and B (unitless), and density (10^{-3} kg cm^{-3}).

	AFCI			ISG			SON68		
	mass%	**mol%**	v_i	**mass%**	**mol%**	v_i	**mass%**	**mol%**	v_i
SiO_2	53.67	58.40	0.251	56.20	60.10	0.263	45.85	52.73	0.214
Na_2O	7.00	7.38	0.052	12.20	12.65	0.091	10.22	11.39	0.076
B_2O_3	9.65	9.06	0.030	17.30	15.97	0.054	14.14	14.03	0.044
Al_2O_3	9.38	6.01		6.10	3.84		5.00	3.39	
CaO	5.00	5.83		5.00	5.73		4.07	5.01	
ZrO_2	1.15	0.61		3.30	1.72		2.75	1.54	
Fe_2O_3	---	0.00		---	0.00		3.03	1.31	
ZnO	---	0.00		---	0.00		2.53	2.15	
Li_2O	4.50	9.85		---	0.00		1.99	4.60	
Nd_2O_3	2.01	0.39		---	0.00		2.04	0.42	
MoO_3	1.50	0.68		---	0.00		1.78	0.85	
Ce_2O_3	1.19	0.24		---	0.00		0.97	0.20	
Cs_2O	1.10	0.26		---	0.00		1.12	0.27	
Others	3.85	1.29		---	0.00		4.51	2.09	
Density	2.78[1]			2.50[2]			2.76[3]		

1 (Crum et al. 2009)

2 (Guerette and Huang 2015)

3 (Gin et al. 2012)

The SON68 and AFCI fabricated at PNNL were made by batching carbonates and oxides, melting the mixtures in a covered platinum crucible for one hour in a furnace, and quenching the melt on a stainless steel plate. The quenched glass was crushed and re-melted for one additional hour to ensure a homogeneous solid. The melt temperature was 1250 °C for SON68 and 1275 °C for AFCI. The quenched glasses were prepared for SPFT by crushing with a tungsten carbide disc mill and sieving the resulting glass powder to a size fraction of 149 µm to 74 µm (- 100 to + 200 mesh). This size fraction was washed and rinsed in both water and ethanol to remove fines following ASTM C1285. Careful sieving and washing of the glass particle is necessary to remove adherent fines on the glass particle surfaces.

The initial surface area, S_0 (m^2), of the glass powder samples is estimated with the geometric formula (McGrail et al. 1997):

$$S_0 = \frac{3m}{\rho r_0} \qquad \text{Eq. 4}$$

where ρ is the glass density (g m^{-3}), m is the mass of the glass powder (g), and r_0 is the average particle radius (m).

2.2 Single-Pass Flow-Through Apparatus

The SPFT system is designed to enable a continuous flow of fresh solution into a vessel containing the material of interest. Collection of the effluent from the vessel allows monitoring of release of elements from the glass as a function of time. A schematic of the SPFT apparatus is shown in Figure 1. A syringe pump (Norgren Kloehn, Las Vegas, NV, USA, Model 55022) is used to draw buffered solution from a reservoir and transfer it at an approximately steady flow rate to the reactor vessels and effluent collection. All connections are made with polytetrafluoroethylene (PTFE) tubing. The 60-mL reactor vessels are Teflon® reactors (Savillex, Minnetonka, MN) with a 40.8-mm inner diameter and 63.6-mm height. Before beginning experiments, the reactors were cleaned with dilute HNO_3 and deionized water according to ASTM C1285. The crushed glass forms a thin layer at the bottom of the reactor, which allows solution contact at the maximum possible surface area. [1]

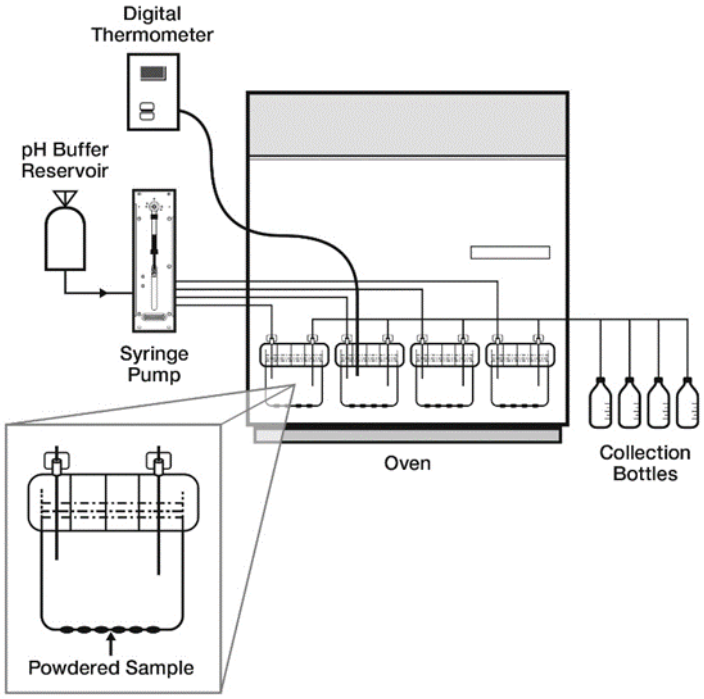

Figure 1. Schematic of the SPFT apparatus for determining reaction rates with a continuously flowing system.

A testing matrix for the SPFT was designed for all three glasses covering a range of temperature (22 °C, 40 °C, 70 °C, and 90 °C) and pH values [pH(22 °C) 9, 10, 11, and 12]. The default test matrix for the various glasses is provided in Table 2. At 40 °C and 90 °C and at each nominal pH(22 °C), five tests were performed where the

[1] Further information on the SPFT technique can be found in ASTM C1662-10.

solution-flow-rate-to-sample-surface-area ratio (q/S) was changed to demonstrate that the systems were approaching the forward rate as q/S values increase. Interpolation of forward rate conditions at the other test temperatures (22 °C and 70 °C) was made based on the results obtained at 40 °C and 90 °C. Unless otherwise noted, only the forward rate measurements are provided in this study.

Table 2. List of SPFT experimental parameters.

Expt. Set	Temp, °C	pH(22 °C)	modeled pH(T)	Test duration, d	q/S × 10^{-8} (m s^{-1})				
1	22	9	8.99	90	2.0	4.0			
2	22	10	9.99	90	2.0	4.0			
3	22	11	11.00	90	2.0	4.0			
4	22	12	12.02	90	2.0	4.0			
5	40	9	8.67	48	1.0	5.0	20	80	200
6	40	10	9.55	48	1.0	5.0	20	80	200
7	40	11	10.89	48	1.0	5.0	20	80	200
8	40	12	11.74	48	1.0	5.0	20	80	200
9	70	9	8.08	28	10	20			
10	70	10	8.88	28	10	20			
11	70	11	10.43	28	10	20			
12	70	12	11.08	28	10	20			
13	90	9	7.72	21	1.0	5.0	20	100	400
14	90	10	8.52	21	1.0	5.0	20	100	400
15	90	11	10.06	21	1.0	5.0	20	100	400
16	90	12	10.70	21	1.0	5.0	20	100	400

During testing, effluent samples were collected at regular intervals. The frequency of sampling intervals depended on the test conditions. Flow rates were determined gravimetrically and the collected effluent was analyzed with inductively coupled plasma optical emission spectroscopy (ICP-OES) for Na, Si, and B. The instrument detection limit for Na, Si, and B was 44.7, 54.8, and 25.2 µg L^{-1}, respectively. The tests were performed until the release of elements from the glass had reached a steady state. For the purposes of this study, a steady-state dissolution rate was defined as three samples collected near the end of the test that did not deviate by more than 15% from their mean value. Steady-state concentrations are provided as the mean value of the last three samples in the given experiment. In certain tests, a coupon of known surface area was added to reduce the overall loss of glass surface area during testing.

2.3 Solution Preparation

The solutions used to control the pH were 0.05 M *tris*(hydroxymethyl)aminomethane (TRIS) [pH(22 °C) 9 and 10] or 0.01 M LiCl [pH(22 °C) 11 and 12] made with deionized water (18.2 MΩ·cm) and adjusted to the desired pH with either 15.8 M HNO_3 or 1 M LiOH. Table 2 includes the computed *in situ* pH of the solution at the various temperatures. The values are taken from Pierce et al. (2008) and were computed from the chemical composition of the buffered solution with the EQ3NR thermodynamic software package (Wolery 1992) as well at with the PHREEQC software package incorporated into the GCMT (Charlton and Parkhurst 2011).

2.4 Dissolution Rate Calculations

In flow-through experiments where a steady-state release of elements has been achieved, the glass dissolution rate indexed to the release of element *i* is calculated with the following equation:

$$r_i = \frac{(C_{i,s} - \overline{C}_{i,b}) \cdot q}{f_i \cdot S} \qquad \text{Eq. 5}$$

where $C_{i,s}$ is the steady-state concentration of element *i* (g m^{-3}) and $\overline{C}_{i,b}$ is the average concentration of element *i* in the blank samples (g m^{-3}). The target concentration are listed in Table 1 along with the values of f_i for the major analytes of interest. The f_i term (unitless) for this study was calculated with the following equation:

$$f_i = mass_i\% \times \left(\frac{mol_i}{mol_{oxide}}\right) \times \left(\frac{MW_i}{MW_{oxide}}\right) \qquad \text{Eq. 6}$$

where $mass_i\%$ is the mass% of the element i^{th} oxide in the glass, mol_i is the moles of element *i* in the oxide, mol_{oxide} is the number of moles of oxide, MW_i is the molecular mass of element *i* (g mol^{-1}), and MW_{oxide} is the molecular mass of the oxide (g mol^{-1}).

An inherent problem with performing dissolution tests under flow-through conditions is the change in the effective surface area as the experiment progresses as glass dissolves and surface area decreases. For this reason, a surface area correction was developed by McGrail et al. (1997) assuming spherical particles of glass. The correction is made through calculation of the mass of glass remaining at each collection interval (*j*), m_j (g):

$$m_j = m_0 - \frac{1}{f_i}\left[\sum_{k=1}^{j-1} q_k C_{k,i} \Delta t_k + q_j C_{j,i} \frac{\Delta t_j}{2}\right], j \geq 1 \qquad \text{Eq. 7}$$

where m_0 is the initial mass of glass (g) and the summation term in the brackets represents the accumulated mass loss up to time step *j*-1. The second term in the brackets represents the average of the total mass loss from time *j*-1 to *j*. The surface area at time *j*, S_j (m^2), can then be calculated with the following expression:

$$S_j = \frac{3}{\rho r_0} m_0^{1/3} m_j^{2/3} \quad \text{Eq. 8}$$

2.5 Experimental Error Calculations

The experimental uncertainty of the glass dissolution rate takes into account uncertainties for each parameter in Eq. 5. For uncorrelated random errors, the standard deviation of a function of the form $f(x_1, x_2, x_n)$ is estimated using the standard, first-order error propagation method:

$$\sigma_f = \sqrt{\sum_{i=1}^{n} \left(\frac{\partial f}{\partial x_i} \right)^2 \sigma_i^2} \quad \text{Eq. 9}$$

where σ_f is standard deviation of the function *f*, x_i is parameter *i*, and σ_i is standard deviation of parameter *i*.

Substitution of Eq. 9 in Eq. 5 and using a relative error, $\hat{\sigma}_{r_i} = \sigma_{r_i} / r_i$, the following equation is obtained:

$$\hat{\sigma}_{r_i} = \sqrt{\left(\frac{\left(\hat{\sigma}_{C_i,s} C_{i,s}\right)^2 + \left(\hat{\sigma}_{\overline{C}_i,b} \overline{C}_{i,b}\right)^2}{\left(C_{i,s} - \overline{C}_{i,b}\right)^2} + \hat{\sigma}_q^2 + \hat{\sigma}_{f_i}^2 + \hat{\sigma}_S^2 \right)} \quad \text{Eq. 10}$$

Relative errors of 10%, 10%, 3%, and 15% are assigned to C_i, $\overline{C}_{i,b}$, f_i, and *S*, respectively. Although the absolute error in f_i is likely higher than 3%, this error is systematic and therefore does not contribute significantly to sample-to-sample uncertainty, which is the principal error of interest here. The 10% for C_i and $\overline{C}_{i,b}$, are the analytical uncertainties. In cases where the elemental concentrations for all three blanks are below the instrument detection, we have made the $\overline{C}_{i,b}$ term equal to the instrument detection limit. The above relative error reflects uncertainty in a single set of experimental measurements but does not reflect uncertainty due to variation in set to set or laboratory to laboratory measurements.

3. RESULTS

3.1 Forward rate determination

At each test temperature and pH combination, upwards of five tests were performed at various q/S values. Conducting the tests at several q/S values ensures that the test parameters necessary to define the forward rate at the test conditions are appropriate. Though we provide the measured release rates of tests at different q/S values at fixed pH and temperature, the focus of this study is on the forward rate values. The implications of rate measurements in flow-through tests where infinitely dilute conditions are not achieved will be discussed in a subsequent paper. The measured effluent concentrations as a function of time are provided in the Supporting Information.

Example of the results of the q/S sweep at 40 °C and 90 °C at pH(22 °C) 9 are provided in Figure 2. The pH(T) is different between these two experiments at different test temperatures so a direct comparison of the B releases from these tests is not possible, however, some general observations merit discussion. In general, the results at 40 °C and 90 °C show that rates at 40 °C are generally an order of magnitude slower than those measured at 90 °C. Additionally, the calculated uncertainties for the 40 °C tests are relatively larger because the solution concentrations are lower in the 40 °C tests than from the 90 °C tests. Lastly, it is observed that the approach to a forward rate occurs at much lower q/S values at the lower temperature. This is the result of lower species concentrations needed to cause solution feedback effects at the lower system temperature.

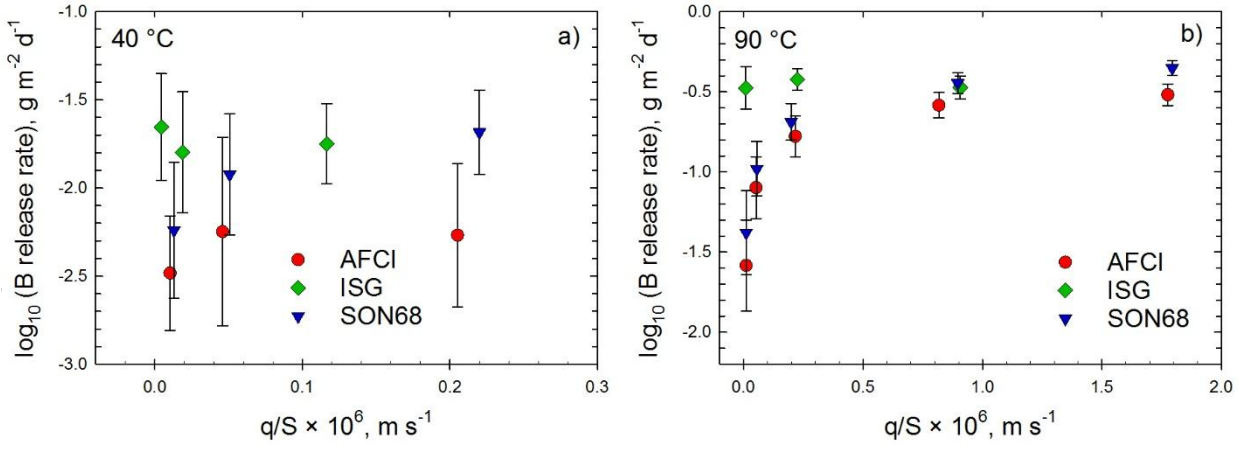

Figure 2. Plot of $\log_{10}$ release rate of boron for three glasses (AFCI, ISG, and SON68) at pH(22 °C) 9 versus the flow-rate-to-sample-surface area ratio (q/S) at a) 40 °C and b) 90 °C. AFCI data point for 40 °C, q/S = 2.16E-07 m s^{-1} based on Si release.

3.2 Forward rate model parameter determination

Table 3 provides the experimental conditions, average steady-state concentrations of B, Na, and Si, and the steady-state forward rates for the three HLW glasses. In general, the release of the three elements from the glass is congruent within uncertainty (2σ ~ 40-50% from Eq. 14). A steady-state was not achieved for the AFCI samples at pH(22 °C) 12 and 90 °C because these corrosion conditions cause rapid changes in surface area, which limited the ability to calculate a steady-state concentration (< 15% r.s.d) for three consecutive samples. To prevent rapid changes in surface area that are intrinsic to tests conducted in these highly corrosive conditions, samples with a lower specific surface area, for instance polished coupons, could be used instead of powder (Icenhower and Steefel 2015). The differences between dissolution rates measured with the use of glass powders have been found agree within experimental uncertainty (Icenhower and Steefel 2015) and by a factor of 1.3 (Fournier et al. 2016). Because of these minimal differences in rates, which are largely within experimental uncertainties, no adjustment to rates measured with the use of powders and coupons was made. The dissolution rates based on the boron concentrations from Table 3 are plotted in Figure 3.

A LMR was performed for these data with a linear representation of Eq. 3:

$$\log_{10}\left(r_{gls}\right)=\log_{10}\left(k_0\right)-\eta\log_{10}\left(a_{H^+}\right)-\frac{1}{2.303}\frac{E_a}{RT} \qquad \text{Eq. 11}$$

A list of the parameters for the glasses studied here, along with values obtained from other studies, is provided in Table 4. Most datasets provided in Table 4 were collected with the SPFT method, however, a few of the datasets were obtained with other test methods. The microchannel test method (Inagaki et al. 2012, Inagaki et al. 2013), similar to the SPFT method, precludes solution recirculation, but the small volume of solution is passed directly over one surface of a glass coupon. The advantage of the microchannel method compared with the SPFT is ease of post-reaction solid analysis and a more precise measurement of surface area. A disadvantage is that the solution may become appreciably concentrated over the short distance of the channel. The Soxhlet test method involves refluxing water, which then condenses and contacts a glass coupon (Delage and Dussossoy 1991). The condensate is collected and analyzed for chemical composition. Both the static test and the modified MCC-1 tests consist of corroding a glass in a static solution with a small surface-area-to-volume ratio (S/V) (Strachan 2001). The difference between the two tests provided in Table 4 is the static tests contain a powder whereas the MCC-1 tests use glass coupons. In

both cases, the forward rate is measured at short time periods before the effect of the concentration of various solution species (principally Si) is encountered.

The various HLW glasses presented in Table 4 are borosilicate glasses that are used to immobilize both simulant (AFCI, ISG, SON68, P0798) and actual (R7T7) waste from used nuclear fuel recycling. The table also includes a subset of HLW glasses from reprocessing in the United Kingdom (Magnox, Magnox-ThORP). The main compositional difference between these glasses and the other HLW glasses is the presence of Mg. Additionally, parameters are provided for a set of low-activity waste (LAW) glasses, whose major compositional difference compared with HLW glasses is a relatively high Na_2O content (~15-25 wt%) and the absence of many rare-earth elements. The interested reader is referred to the references in Table 4 for a complete description of the various glass compositions.

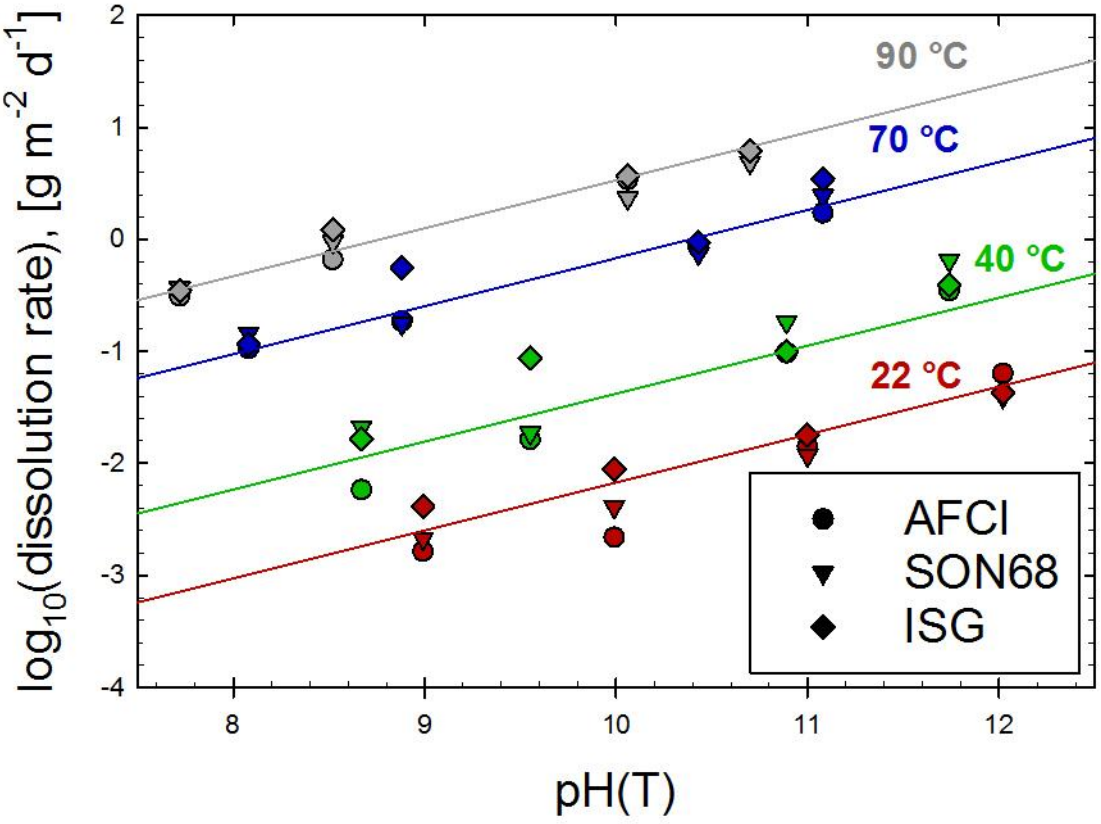

Figure 3. Normalized boron release rates as a function of pH(T) and temperature for AFCI, ISG, and SON68. The solid lines are the result of the linear regression for the SON68 data.

Table 3. SPFT experimental conditions, average steady-state effluent concentrations, and steady-state dissolution rates based on B, Na, and Si for AFCI, ISG, and SON68.

Glass	Temp °C	pH(22 °C)	Test flow rate $m^3\ d^{-1}$	surface area at steady state m^2	steady-state [B] ug L^{-1}	steady-state [Na] ug L^{-1}	steady-state [Si] ug L^{-1}	steady-state rate, B g $m^{-2}\ d^{-1}$	steady-state rate, Na g $m^{-2}\ d^{-1}$	steady-state rate, Si g $m^{-2}\ d^{-1}$
AFCI	23	9	3.89E-05	2.00E-02	<2.52E+01	<4.46E+01	1.27E+02	<1.64E-03	<1.68E-03	9.86E-04
		10	2.11E-05	9.56E-03	2.97E+01	5.56E+01	2.37E+02	2.19E-03	2.37E-03	2.09E-03
		11	1.84E-05	5.01E-03	1.15E+02	1.78E+02	9.27E+02	1.40E-02	1.26E-02	1.35E-02
		12	1.73E-05	4.69E-03	5.19E+02	9.82E+02	4.41E+03	6.37E-02	6.96E-02	6.46E-02
	40	9	1.62E-05	3.95E-03	4.24E+01	9.48E+01	3.49E+02	5.82E-03	7.50E-03	5.72E-03
		10	3.52E-05	3.80E-03	5.30E+01	1.02E+02	4.82E+02	1.64E-02	1.82E-02	1.78E-02
		11	2.00E-05	6.15E-04	8.97E+01	2.08E+02	1.03E+03	9.73E-02	1.31E-01	1.34E-01
		12	7.83E-05	7.47E-04	9.98E+01	6.75E+02	9.95E+02	3.49E-01	1.36E+00	4.15E-01
	70	9	2.48E-05	4.33E-04	5.58E+01	<4.46E+01	4.84E+02	1.07E-01	<4.94E-02	1.11E-01
		10	3.99E-05	1.12E-03	1.56E+02	2.51E+02	1.35E+03	1.86E-01	1.73E-01	1.93E-01
		11	3.95E-05	1.89E-03	1.22E+03	2.17E+03	1.07E+04	8.54E-01	8.74E-01	8.88E-01
		12	2.37E-05	3.94E-04	8.59E+02	1.79E+03	7.51E+03	1.73E+00	2.08E+00	1.80E+00
	90	9	1.50E-04	8.86E-04	5.54E+01	9.04E+01	5.20E+02	3.12E-01	2.94E-01	3.50E-01
		10	1.26E-04	8.56E-04	1.35E+02	2.02E+02	1.13E+03	6.62E-01	5.74E-01	6.63E-01
		11	7.44E-05	7.51E-04	1.04E+03	1.86E+03	8.51E+03	3.43E+00	3.55E+00	3.36E+00
		12	Steady-state conditions not achieved							
ISG	23	9	2.95E-05	1.07E-02	8.02E+01	1.11E+02	3.68E+02	4.13E-03	3.38E-03	3.87E-03
		10	1.84E-05	5.51E-03	1.42E+02	2.55E+02	6.75E+02	8.82E-03	9.39E-03	8.58E-03
		11	2.03E-05	5.72E-03	2.71E+02	4.49E+02	1.31E+03	1.79E-02	1.76E-02	1.77E-02
		12	5.68E-06	5.31E-03	2.13E+03	3.31E+03	1.00E+04	4.25E-02	3.92E-02	4.09E-02
	40	9	3.98E-05	4.23E-03	9.42E+01	1.94E+02	5.02E+02	1.65E-02	2.02E-02	1.80E-02
		10	3.63E-05	1.06E-03	1.37E+02	2.53E+02	7.26E+02	8.74E-02	9.57E-02	9.48E-02
		11	7.77E-05	1.09E-03	<7.56E+01	3.21E+02	9.22E+02	<1.00E-01	2.52E-01	2.50E-01
		12	1.96E-05	5.47E-04	5.83E+02	1.33E+03	3.66E+03	3.89E-01	5.26E-01	5.00E-01
	70	9	2.73E-05	5.44E-04	1.26E+02	8.84E+01	1.08E+02	1.18E-01	4.90E-02	2.06E-02
		10	3.61E-05	1.12E-03	9.36E+02	1.63E+03	4.74E+03	5.60E-01	5.78E-01	5.80E-01

Glass	Temp °C	pH(22 °C)	Test flow rate $m^3\ d^{-1}$	surface area at steady state m^2	steady-state [B] $ug\ L^{-1}$	steady-state [Na] $ug\ L^{-1}$	steady-state [Si] $ug\ L^{-1}$	steady-state rate, B $g\ m^{-2}\ d^{-1}$	steady-state rate, Na $g\ m^{-2}\ d^{-1}$	steady-state rate, Si $g\ m^{-2}\ d^{-1}$
		11	3.73E-05	1.85E-03	2.52E+03	4.55E+03	1.25E+04	9.44E-01	1.01E+00	9.55E-01
		12	7.97E-05	2.62E-04	6.15E+02	1.13E+03	3.22E+03	3.48E+00	3.78E+00	3.72E+00
	90	9	3.88E-05	1.88E-03	9.10E+02	1.68E+03	1.95E+03	3.50E-01	3.84E-01	1.54E-01
		10	3.98E-05	1.47E-03	2.42E+03	4.43E+03	1.20E+03	1.22E+00	1.32E+00	1.23E+00
		11	7.04E-05	7.44E-04	2.10E+03	3.72E+03	9.54E+03	3.69E+00	3.89E+00	3.44E+00
		12	3.61E-05	9.22E-04	8.46E+03	1.56E+04	3.99E+04	6.17E+00	6.75E+00	5.95E+00
SON68	23	9	3.56E-05	9.55E-03	<2.52E+01	<4.46E+01	1.03E+02	<2.13E-03	<2.16E-03	1.78E-03
		10	1.80E-05	9.61E-03	9.63E+01	1.65E+02	4.45E+02	4.10E-03	4.06E-03	3.88E-03
		11	1.92E-05	4.78E-03	1.29E+02	2.07E+02	6.07E+02	1.18E-02	1.09E-02	1.14E-02
		12	2.89E-05	4.90E-03	2.95E+02	5.41E+02	1.58E+03	3.95E-02	4.21E-02	4.33E-02
	40	9	3.80E-05	1.94E-03	4.74E+01	8.41E+01	2.66E+02	2.12E-02	2.18E-02	2.43E-02
		10	3.60E-05	2.08E-03	4.72E+01	1.22E+02	3.50E+02	1.86E-02	2.79E-02	2.83E-02
		11	6.02E-05	8.78E-04	1.18E+02	2.54E+02	5.40E+02	1.83E-01	2.29E-01	1.72E-01
		12 [a]	1.55E-04	4.67E-04	8.59E+01	6.60E+02	4.83E+02	6.51E-01	2.90E+00	7.50E-01
	70	9	3.07E-05	4.07E-04	8.50E+01	<1.34E+02	4.38E+02	1.46E-01	<1.33E-01	1.54E-01
		10	3.64E-05	1.28E-03	2.73E+02	4.93E+02	1.42E+03	1.77E-01	1.85E-01	1.89E-01
		11	3.91E-05	1.83E-03	1.54E+03	2.82E+03	7.43E+03	7.51E-01	7.94E-01	7.41E-01
		12	7.60E-05	2.78E-04	3.94E+02	7.35E+02	2.09E+03	2.45E+00	2.65E+00	2.67E+00
	90	9	8.08E-05	9.70E-04	1.93E+02	3.63E+02	9.51E+02	3.67E-01	3.99E-01	3.69E-01
		10	1.62E-04	8.64E-04	2.23E+02	2.48E+02	1.05E+03	9.52E-01	6.13E-01	9.20E-01
		11	8.11E-05	6.69E-04	8.44E+02	1.43E+03	3.73E+03	2.33E+00	2.28E+00	2.11E+00
		12	3.76E-05	7.99E-04	4.52E+03	1.00E+04	2.10E+04	4.85E+00	6.22E+00	4.61E+00

[a] High sodium and silicon background for this reactor.

Table 4. A list of rate model parameters for several glasses. The parameter values populate Eq. 3 to calculate the glass dissolution rate as a function of temperature and pH. The composition of each glass is provided in the Supporting Information.

	Glass Type	$\log_{10} k_0$ (g m^{-2} d^{-1}) [a]	η	E_a (kJ mol^{-1})	R^2	Reference	Method	Note
AFCI	HLW	8.3 ± 0.5	0.51 ± 0.03	90 ± 3	0.99	Present study	SPFT	
ISG	HLW (simplified SON68)	8.3 ± 0.6	0.39 ± 0.04	80 ± 4	0.97	Present study	SPFT	
		---	0.23	77	---	(Inagaki et al. 2013)	Microchannel	E_a at pH 10. Values reported in Ref.
		7.9 ± 0.7	0.22 ± 0.02	65 ± 4	0.96	(Inagaki et al. 2013)		Fit performed in present study
SON68	HLW (R7T7 simulant)	8.2 ± 0.7	0.43 ± 0.05	83 ± 5	0.96	Present study	SPFT	
		8.1	0.4 ± 0.1	76 ± 5	---	(Frugier et al. 2008)	Soxhlet	
R7T7	HLW	---	---	59 ± 2	---	(Delage and Dussossoy 1991)	Soxhlet	
		---	0.41 ± 0.02	---	---	(Advocat et al. 1991)	Static	
P0798	HLW			76		(Inagaki et al. 2012)	Microchannel	E_a at pH 10. As reported in Ref.
		7.1 ± 0.9	0.30 ± 0.05	66 ± 5	0.96	(Inagaki et al. 2012)	Microchannel	Fit performed in present study
SRL202	HLW	8.3 ± 1.0	0.56 ± 0.07	93 ± 7	0.94	(Pierce et al. 2008)	SPFT	Fit performed in present study
LD6-5412	LAW	7.0 ± 0.5	0.40 ± 0.03	74.8 ± 1.0	0.97	(McGrail et al. 1997)	SPFT	Based on Si.
MT25	HLW (Magnox-ThORP	9.4 ± 1.2	0.48 ± 0.05	88 ± 7	---	(Cassingham et al. 2015)	SPFT	Fit performed in present study
MT30	HLW (Magnox-ThORP)	7.8 ± 1.1	0.50 ± 0.05	80 ± 7	---	(Cassingham et al. 2015)	SPFT	Fit performed in present study
MW glass	HLW (Magnox)	---	0.43 ± 0.07	64		(Abraitis et al. 2000)	modified MCC-1	E_a value at pH 12.1
MW25	Magnox			59.6		(Iwalewa et al. 2017)	SPFT	
LAWABP1	LAW	6.5	0.35 ± 0.03	68 ± 3.0	NA	(McGrail et al. 2001a)	SPFT	
LAWA44	LAW	4.1	0.49 ± 0.08	60 ± 7	0.78	(Pierce et al. 2004)	SPFT	
LAWB45	LAW	4.2	0.34 ± 0.03	53 ± 3	0.90	(Pierce et al. 2004)	SPFT	
LAWC22	LAW	5.0	0.42 ± 0.02	64 ± 2	0.98	(Pierce et al. 2004)	SPFT	

	Glass Type	$\log_{10} k_0$ (g m^{-2} d^{-1}) [a]	η	E_a (kJ mol^{-1})	R^2	Reference	Method	Note
ORPLB2	LAW	4.7	0.49 ± 0.05	58 ± 3	0.98	(Papathanassiu et al. 2011)	SPFT	
IDF18-A161	LAW	6.8 ± 0.9	0.28 ± 0.06	61 ± 6	0.89	(Neeway et al. 2017)	SPFT	
ORPLG9	LAW	8.4 ± 1.0	0.36 ± 0.07	81 ± 7	0.91	(Neeway et al. 2017)	SPFT	
NeB1	5-component		0.49 ± 0.24			(Pierce et al. 2010)	SPFT	
NeB2	5-component		0.50 ± 0.15			(Pierce et al. 2010)	SPFT	
NeB3	5-component		0.46 ± 0.18			(Pierce et al. 2010)	SPFT	
CSG[b]	HLW (Simplified SRL-165)	5.6 ± 1.0	0.49 ± 0.03	75 ± 6	0.96	(Knauss et al. 1990)	SPFT	Based on Si. Fit performed in present study
			0.47 ± 0.05			(Knauss et al. 1990)		Average of η values reported in Ref.

Note: All values based on boron unless otherwise stated

[a] Values have been converted from k_0 to $\log_{10} k_0$ where necessary. Uncertainties reported if provided in parent document

[b] The glass was originally reported as a "5-component" glass (Knauss et al. 1990). CSG is the more common name for the glass (Jeong and Ebert 2002).

3.3 Uncertainty analysis of forward rate model parameters provided with a nonlinear multivariate regression

The GCMT was used to fit the boron experimental data provided in Section 3.2 for AFCI, ISG, and SON68. The GCMT is a tool that consists of a set of software packages including differential equation solver, chemistry package solvers, and parameter optimization solvers that communicate through a MatLab interface. PhreeqC (Charlton and Parkhurst 2011) was used for the determination of pH buffer values. The GCMT relies on principle component analysis (PCA) analysis (Bro and Smilde 2014) of the SPFT data to generate confidence interval ellipsoids. PCA is used in a wide number of applications but is primarily intended to reduce the "dimensionality" of a set of data by determining the principle components (PC) as linear combinations of the original variables and then eliminating those PCs that have minor influence on the understanding of the data. The PEST software package (Doherty 2015) was used to find the optimal parameter fit and to obtain information needed for further statistical analysis of the parameter uncertainty.

Table 5 provides a comparison of the mean values calculated both through the LMR method and through the nonlinear multivariate regression used with the GCMT. Use of the LMR and GCMT methods results in similar mean values within one standard deviation. To obtain the values shown in Table 5, the assumption is made that the parameter values are uncorrelated. However, as shown below, this is not the case.

Table 5. Mean values and standard deviations calculated using the LMR and GCMT method. Uncertainties are one standard deviation.

Glass	AFCI			ISG			SON68		
Parameter	η	E_a kJ mol^{-1}	$\log_{10}(k_0)$ [g m^{-2} d^{-1}]	η	E_a kJ mol^{-1}	$\log_{10}(k_0)$ [g m^{-2} d^{-1}]	η	E_a kJ mol^{-1}	$\log_{10}(k_0)$ [g m^{-2} d^{-1}]
LMR	0.51 ± 0.03	90 ± 3	8.3 ± 0.5	0.39 ± 0.04	80 ± 4	8.3 ± 0.6	0.43 ± 0.05	83 ± 5	8.2 ± 0.7
GCMT	0.50 ± 0.03	90 ± 3	8.5 ± 0.5	0.38 ± 0.04	81 ± 4	8.5 ± 0.5	0.44 ± 0.04	85 ± 4	8.4 ± 0.7

A non-linear, iterative multivariate fit of the data is used in the GCMT to minimize the squares of the weighted residuals – the Φ value – commonly referred to as the objective function. It is not conceptually different than the LMR method used in Section 3.2, except that a Jacobian-based algorithm is used in the GCMT to determine a path through parameter space to arrive at the best estimate of the parameters required by a particular model. The GCMT attempts to minimize the value of Φ given by:

$$\Phi = \sum_i \left(w_i \left(O_i^{\exp} - O_i^{\mathrm{mod}} \right) \right)^2 \qquad \text{Eq. 12}$$

where w_i is the weight assigned to a particular experimental observable, $O_i^{\exp}$ is the experimental observable, and $O_i^{\exp}$ is the model prediction of the observable value. For these datasets, both reciprocal and unit weighting were tested.

Table 6 shows the correlation coefficient matrix for the AFCI glass. For uncorrelated parameters the off-diagonal terms should be zero and from -1.0 to 1.0 for correlated parameters. As reported in Table 5 above, the LMR analysis provides only the standard deviation while the values for the GCMT analysis were taken from the diagonal values of the covariance matrix output by the PEST subroutine. Clearly the parameters are significantly correlated and the standard deviation values of Table 5 are insufficient to completely characterize the uncertainty in the parameters as it is not possible to independently vary each parameter individually without resulting in an unrealistic parameter space that reproduces experimental data. Analysis of ISG and SON68 data showed similar parameter correlations. The covariance matrix can be used to perform a Principle Component Analysis (Everitt and T. 2011), which entails determining the Eigenvectors and Eigenvalues of the best fit residual and using these vectors to generate ellipses in 2D or ellipsoids in 3D, which provide a visual representation of uncertainties in parameter space.

Table 6. Correlation Coefficient Matrix for AFCI.

	η	E_a	$\log_{10}(k_0)$
η	1.00	0.47	-0.12
E_a	0.47	1.00	0.81
$\log_{10}(k_0)$	-0.12	0.81	1.00

Two-dimensional maps of the Φ function allow visualization of where the minimum value of Φ lies and how sensitive it is to small changes, therefore offering another method for understanding parameter correlation. The results of these Φ maps for AFCI are presented in Figure 4. The mean values of the GCMT analysis (blue) and the LMR analysis (green) are plotted and the reader should note that the uncorrelated standard deviation values are relatively large compared to the region plotted. The 2D colored contours represent values of Φ for a given set of parameters values with one value fixed. The contour minima and the calculated parameter mean do not quite match but this is an artifact of the algorithm termination criteria and the necessity of slicing 3D space into 3 planes for 2D

representation. In this instance, the LMR analysis gave a mean value slightly closer to the Φ minimum than the GCMT but the differences are insignificant and for other glasses the trend was reversed. The figures demonstrate the appearance of a "trough" along which the Φ does not vary greatly and provide a graphical representation of correlation. A change in one parameter requires a corresponding change in the other parameters to remain within an acceptable range of Φ values. In summary, the standard deviations for the rate parameters presented in Table 5 are somewhat misleading as all parameters in the rate model must be simultaneously varied if an accurate reproduction of the experimental data is desired.

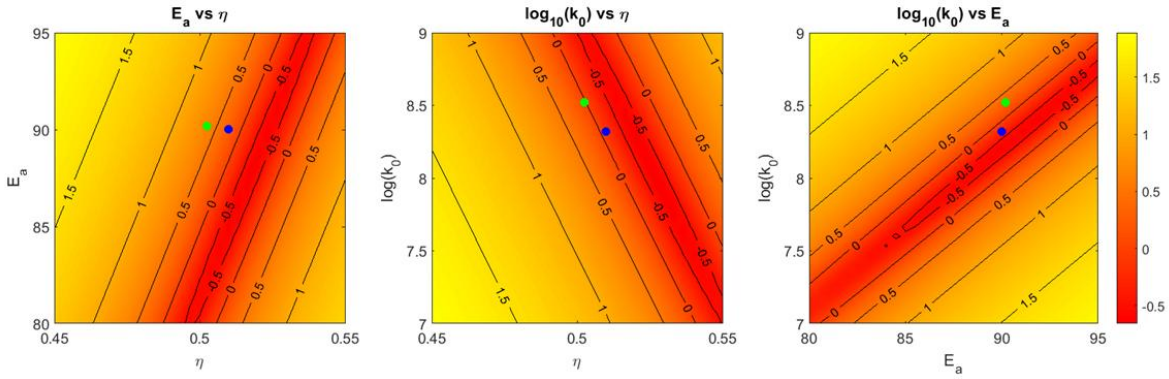

Figure 4. The optimization function (Φ) maps of each parameter pair for the AFCI glass. The green points are the values found with the GCMT to fit the data and the blue points are those obtained with the LMR method. The contour values are the $\log_{10}(\Phi)$.

Figure 5 is an extension of the Φ maps of Figure 4 into 3D space and adds results for the other two glasses tested here (ISG and SON68). The ellipses presented in Figure 5 are the 95% confidence interval volumes. The large dot in Figure 5 is the mean value though the size of the dot is only intended to enhance the visualization of the data. In the 3D space, it is seen that the parameters are highly correlated and cannot be varied independently without risk of falling outside of the 95% confidence interval. It is also evident that the ellipses are nearly flat (i.e. 2D). The "flatness" of these ellipses is discussed in Section 4.4. The 95% confidence interval ellipsoids overlap significantly and the ISG mean values are insignificantly different from those for SON68 or AFCI. However, SON68 and AFCI appear to be marginally different.

Because all the ellipsoids are nearly planar, it would be possible to describe the relationship between the parameters as a plane bounded by an ellipse. With the choice of two parameters, the third will be fixed and could be calculated. This would significantly constrain the selection of acceptable parameters combinations. The use of the

standard deviations listed in Table 5, where no parameter correlation is assumed, would result in selection of parameters combination from a 3D rectangular space and allow unrealistic parameter combinations to be used.

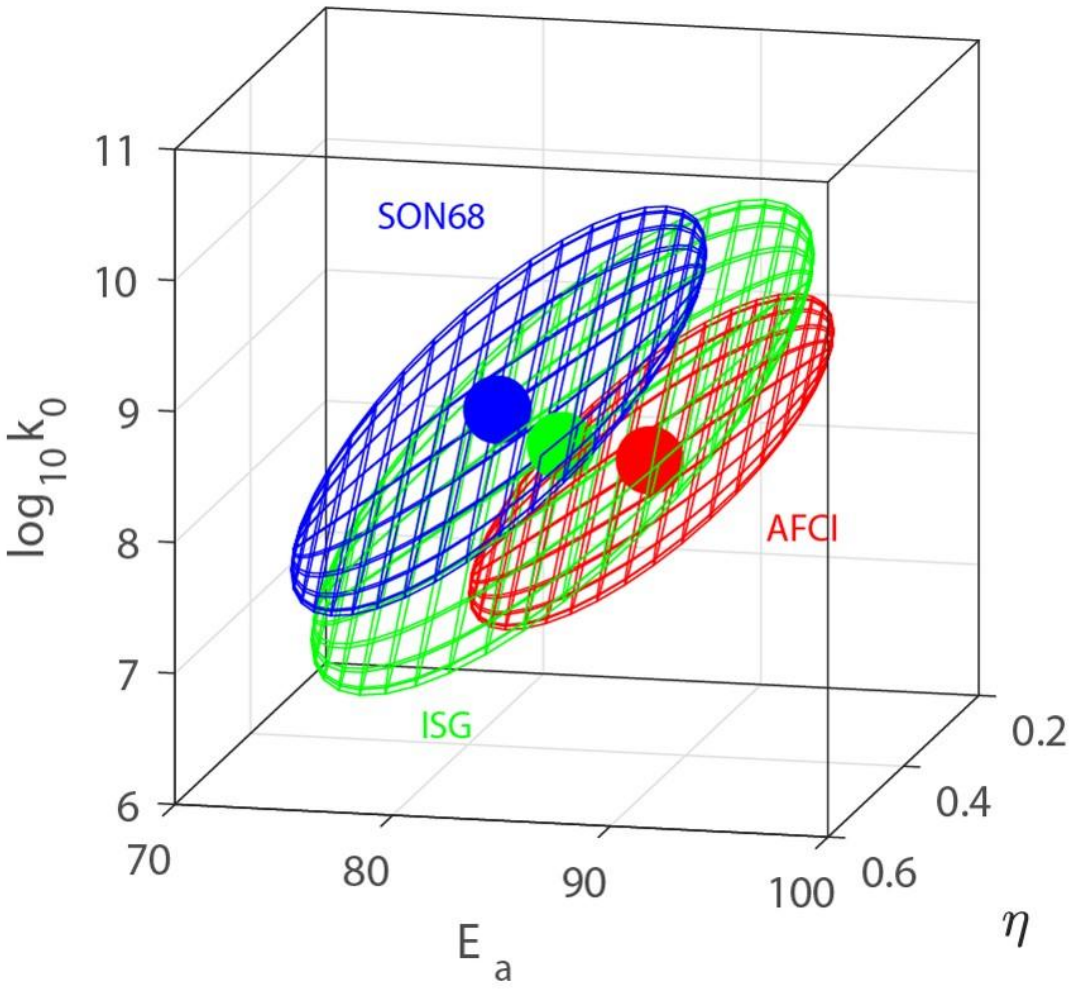

Figure 5. Plot of mean rate parameter values for AFCI, ISG, and SON68 (solid dots) along with ellipses representing the 95% confidence interval. Unlike the ellipsoids, the size of the mean value dots was chosen for visual clarity and not meant to represent any confidence interval.

4. Discussion

4.1 Relative durability of AFCI, ISG, and SON68

In terms of the behavior of the different glasses, two distinct dissolution behaviors are observed. For SON68 and AFCI, the dissolution rate (see Figure 2) initially increases rapidly but approaches a near constant value at high q/S values where the forward dissolution rate can be determined. Over the investigated q/S range and at pH(22 °C) 9, the mean dissolution rate of SON68 is 3.7 times faster than the mean dissolution rate of AFCI at 40 °C and 1.2

times faster than the dissolution of AFCI at 90 °C. In contrast to AFCI and SON68, ISG dissolves at a rate that appears to be equivalent within the range of experimental error for the investigated q/S ratios. This behavior has been observed for a phase separated glass where one phase, likely $Na_2B_4O_7$ dissolved out of the surface, leaving a pattern of aligned, elliptically-shaped pits in the residual matrix rich in Si and Al (Icenhower et al. 2003). Though the dissolution rate of ISG is unaffected by changes in the saturation state of the system, the glass dissolution rate for ISG does have a dependence both on temperature and pH and an effort can be made to fit rate model parameters for this glass. Therefore, determination of rate model parameters for this glass is possible. Over the investigated q/S range and at pH(22 °C) 9, the dissolution rate of ISG is 0.9 times the mean dissolution rate of SON68 at 40 °C and 1.1 times faster than the mean dissolution rate of SON68 at 90 °C. In contrast, Gin et al. (2012) showed the forward dissolution rate of SON68 was 1.3 times faster than CJ4 (a glass with the same nominal composition as ISG) for static dissolution tests buffered at pH 9 at 90 °C with a glass-surface-area-to-solution-volume ratio of 10 m^{-1}.

4.2 Note on Rate Parameter Determination

To obtain the mean parameter values presented in Table 5, a regression was performed across the entire data set and all three rate model parameters were solved simultaneously. This is not always the method performed in some studies reported in the literature. Some investigators have evaluated glass dissolution data sets to obtain the activation energy and pH-dependent parameters separately performing two regressions: one to determine the apparent activation energy, E_a, and another to determine the pH-dependent parameter, η (Cassingham et al. 2015, Pierce et al. 2008). A linear regression with a variant of Eq. 11 is first performed at a variety of pH values to obtain E_a from the slope. The remaining intercept value can then be fit with a second linear regression to obtain the η value from the slope and the k_0 values from the intercept. A global fit of the boron data leads to more robust uncertainty calculations because it allows for a calculation of coefficients without ignoring possible correlation among data and coefficients that may occur if the various parameters were to be fit separately. Evidence of correlation between the parameters has been demonstrated in the present work.

The value of k, reported by Cassingham et al. (2015) and Pierce et al. (2008) as the forward rate constant, should not be confused with k_0 (also given as $\bar{k}$ in the literature) used in this work as it includes both the k_0 and activation energy terms in Eq. 3. Without consideration of the meaning of k_0 the glass dissolution rate can vary by orders of magnitude. Thus, to provide the comparable set of rate model parameters provided in Table 4, where

possible, we have used rates reported in the referenced papers and performed our own fits to solve for the rate model parameters that may be used in Eq. 3.

4.3 Comparison to Dissolution Rates in the Literature

For SON68, the majority of data available in the literature for the forward rate of dissolution near pH(22 °C) 9 and 90 °C range between 0.89 and 5.5 m^{-2} d^{-1} (Frugier et al. 2008, Jegou et al. 2000). As noted by Icenhower and Steefel (2013), these high dissolution rates may be the result of the test conditions under which the data were obtained, specifically if the tests are performed in static conditions. More recent studies by Jollivet et al. (2012) and Icenhower and Steefel (2013) in flow-through conditions have reported forward dissolution rate values of 0.33 g m^{-2} d^{-1} [pH(25 °C) 7.45] and 0.55 g m^{-2} d^{-1} [pH(22 °C) 9][2], respectively, which is in agreement with the value reported from the present study.

It is also possible to compare the results obtained for ISG in the present study with other data available in the literature. Interpolating the results from Inagaki et al. (2013), the dissolution rate of ISG measured with a microchannel apparatus at 90 °C, pH(T) 10 was 7.94 g m^{-2} d^{-1}. The results from Fournier et al. (2016) ranged from 10.59 - 16.98 g m^{-2} d^{-1} with static tests, 9.58 - 13.03 g m^{-2} d^{-1} with the microchannel, and 17.11 - 16.28 × 10^{1} g m^{-2} d^{-1} with the flow-through column. Compared to ISG dissolution rate of 5.44 g m^{-2} d^{-1} at 90 °C and pH(22 °C) 11 obtained in the present study, the dissolution rates from Inagaki et al. (Inagaki et al. 2013) and Fournier et al (2016) are factors of 1.8 to 3.1 faster, respectively. The rates measured with the microchannel apparatus show better agreement with the SPFT reported here.

The difference in the buffer solutions used also deserves to be highlighted. In the present study, a solution of 10^{-2} m LiCl was adjusted to the desired test pH with the addition of LiOH, while (Inagaki et al. 2013) used a 10^{-3} M KCl solution adjusted to the desired pH with KOH and Fournier et al (2016) did not use a chloride salt and simply adjusted to the desired pH with KOH. Neeway et al. (2016) highlighted the disparate behavior in the interdiffusion of Li^{+} and K^{+} into simulant glasses based on the ISG composition. This may create a situation where different chloride salts affect the surface composition of the glass and lead to different dissolution rates. Because it has been

[2] The value reported in Icenhower and Steefel (2013) is actually 0.30 g m^{-2} d^{-1}. However, that value was incorrectly reported because the incorrect value of f_B was used. The value of 0.55 g m^{-2} d^{-1} was recalculated from the values reported in their Tables 4 and 5.

shown that the choice of buffer may affect the glass dissolution rate (Tournié et al. 2013), the effect of buffer system on measured glass dissolution rates may also be responsible for differences in reported rates.

The differences in measured rates may be attributed to the various experimental methods and lab-to-lab variations in experimental results. Though identification of the reasons for differences in measured dissolution rates with the use of different testing methods is important, these uncertainties are ignored from the rate parameter modeling fits presented in Section 4.4.

4.4 Comparison of Rate Model Parameters to Literature Values

Table 4 shows a range of rate model parameters for a set of simulant nuclear waste glasses; k_0 ranges from 1.3×10^4 to 2.6×10^9 g m^{-2} d^{-1}, η ranges from 0.22 to 0.56, and E_a ranges from 53-90 kJ mol^{-1}. The parameter k_0 is often referred to as the intrinsic rate constant as it is intrinsic to the glass composition and independent of solution composition and temperature (Strachan 2001). However, care should be taken in fitting this parameter because, as will be explained below, k_0 and E_a may be highly correlated during the fitting exercise. Thus an equally good fit to the data may be achieved when an increase in k_0 is accompanied by an increase in E_a (note the E_a parameter is present as the negative in the exponential term), or vice versa.

The next term of interest is the η term, which is the order of reaction with respect to $[H^+]$. Because of the importance of the pH dependence of the dissolution reaction, the product term in Eq. 1 is often simplified to include only the hydrogen ion activity term and all other factors are ignored. The importance of pH on the glass dissolution reaction is related to the sorption of H^+, H_2O, and OH^- on the glass surface (Zapol et al. 2013). For this reason, separate parameter values for the pH dependency have been proposed for use in acidic, neutral, and alkaline solutions (Köhler et al. 2003). In the alkaline range, the values in Table 4 show η values ranging from 0.22-0.56. A question that arises from this observation is why a fractional value is obtained (i.e. $0 < \eta < 1$). One possible reason was provided by Lasaga (1995) who proposed that the reason for the fractional value is that the dependence of the rate is not related to the bulk pH (i.e. solution activity of H_3O^+) but rather to the activity of H_3O^+ on the surface.

It should be noted that many glasses and minerals exhibit a V-shaped dependence in the dissolution rate as a function of pH, i.e. the rate is relatively high in acids, approaches a minimum in the near-neutral pH range, and increases in as the alkalinity of the solution increases (Brantley 2008). Some authors have approached this observed

behavior by merely changing the sign of η in Eq 4 as conditions change from alkaline to acidic, but the slope of glass dissolution as a function of pH is not equal for acidic and alkaline solutions (Inagaki et al. 2012, Inagaki et al. 2013, Knauss et al. 1990). Thus the simple change in sign on the η term may not be appropriate and glass dissolution should be studied across a wider pH range in order to have a more fundamental understanding of the glass dissolution process. In addition to a discussion of the roles of OH^- and H_3O^+ on controlling the glass dissolution rate, the use of a rate model with a neutral water species has also been proposed to explain mineral dissolution rates (Köhler et al. 2003) and extended to glass by Strachan (2017). These observations merit further study for a more complete explanation of glass dissolution across the entire pH range. However, for the purposes of this study, where the role of pH in the alkaline range is studied because those are the conditions expected in a geological repository, the η terms provided in Table 4 are appropriate for this discussion. Even if the rate equation is shown to be similar to that of (Köhler et al. 2003), the experimental value of η should be the same, since it is the slope of the dissolution rate with pH.

The range of E_a values from 53-90 kJ mol^{-1} is consistent with ranges determined experimentally and calculated for silicates and basaltic glasses (Criscenti et al. 2006, Dove 1999, Icenhower and Dove 2000, Rimstidt and Barnes 1980, Wolff-Boenisch et al. 2004). Some studies report activation energies at fixed pH where temperature is varied (Inagaki et al. 2012, Inagaki et al. 2013, Knauss et al. 1990). The activation energies are calculated on both the alkaline and acidic side. Changes in activation energies as changes in pH occur would indicate that the mechanism of glass alteration changes with changing pH. For the fits performed in this paper, our focus is on dissolution data where a linear behavior between pH and log dissolution rate is observed. This generally occurs at near-neutral to alkaline conditions. At these pH values, the hydrolysis reaction is mediated by the relatively high concentration of solution OH^-.

The values listed in Table 4 are apparent activation energies because several elementary reactions may be involved in the dissolution of these complex glasses. Activation energies in the range presented here are typically associated with the rupture of Si-O-Si bonds. This is because they are too high to be associated with a diffusion-controlled process (Strachan 2001), where apparent activation energies are found to be in the order of 30-50 kJ/mol (McGrail et al. 2001b, Ojovan et al. 2006, Shutthanandan et al. 2002). As noted by Neeway et al. (2016), if the diffusion-controlled reaction is ion-exchange/interdiffusion between H^+ or H_3O^+ and alkali in the glass, including a

chemical reaction involving the dissociation of O-H bonds must be occurring as the alkali-alkali ion-exchange/interdiffusion process results in activation energies between 100 to 150 kJ mol^{-1}. For the three glasses investigated in this study, where possible variations in glass dissolution rate measurements that can be attributed to different test methodologies have been largely eliminated, the range in activation energies is quite small (81-90 kJ mol^{-1}). This suggests that the differences between these HLW glass compositions have a minimal effect on the rate-limiting step in the glass-water reaction.

The various rate model parameters compiled from the literature and presented in Table 4 are plotted in Figure 6. Both LAW (red) and HLW (green) glasses as well as the HLW glasses from this study (blue) are plotted. For comparison, Figure 6a shows the 95% confidence interval for the HLW glasses AFCI, SON68, and ISG along with the 95% confidence interval for three LAW glasses: LAWA44, LAWB45, and LAWC22 (Pierce et al. 2008). In comparison to the HLW glasses studied in the present paper, the ellipses generated from LAWA44, LAWB45, and LAWC22 are centered on lower k_0 and E_a values. Though the 95% confidence ellipse of LAWA44, LAWB45, and LAWC22 overlap with those of SON68 and ISG, only LAWA44 is shown to overlap with the 95% confidence ellipse of AFCI. In general for the whole dataset, the mean HLW parameter values appear to cluster in a high E_a/high k_0 area while the LAW glasses appear to cluster in a low E_a/low k_0 area. At present, we are unable to identify the underlying kinetic phenomenon for the differences in location of rate model parameters in the 3D plot but a simple explanation would be due to the higher alkali concentration of the LAW glasses.

Figure 6b is a rotation of Figure 6a and shows that all the points fall roughly on a plane through the parameter space. The ellipsoid planes for each of the glasses are parallel and align in a single plane. These results suggest that each glass can be described by the two largest rate parameters as a 2D ellipse and that the original TST parameters can be described as a linear combination of the two largest parameters. The correlation between the TST parameters indicates the model can be reduced to two variables. The details of this would require some analysis, though it may be possible to describe the dissolution of a particular glass by the selection of two TST parameters and calculate the third based upon a linear algebraic relationship common to all glasses, which would result in a robust model with fewer parameters.

As explained above, with the high degree of correlation between parameters, an equally good fit to the data may be achieved when an increase in k_0 is accompanied by an increase in E_a, or vice versa. This is a significant drawback

to the two step regression fitting method described in Section 4.2 as it may skew the relationship between the parameters. Assuming, however, that the points in Figure 6 are reasonably independent of the method of fitting, it is clear that glass composition has a significant influence on the rate parameters and the difference cannot be explained by experimental uncertainty. The LAW glasses are distinct from HLW glasses based upon the k_0 and E_a values and within each of these groups there are probably significant differences in the best fit model parameters. On the other hand, the η values appear to fluctuate independently of its designation as an HLW or LAW glass. These relationships bring forth the possibility of directly relating glass composition to model parameters. One possible approach to understand and quantify compositional changes would include systematic variations of the glass composition. This strategy has been used by some investigators where changes in the glass dissolution rate were directly correlated with changes in the glass structure as compositional changes were made (Angeli et al. 2008, Bergeron et al. 2010, Cailleteau et al. 2008, Davis et al. 2003, Hopf et al. 2016, Pierce et al. 2010).

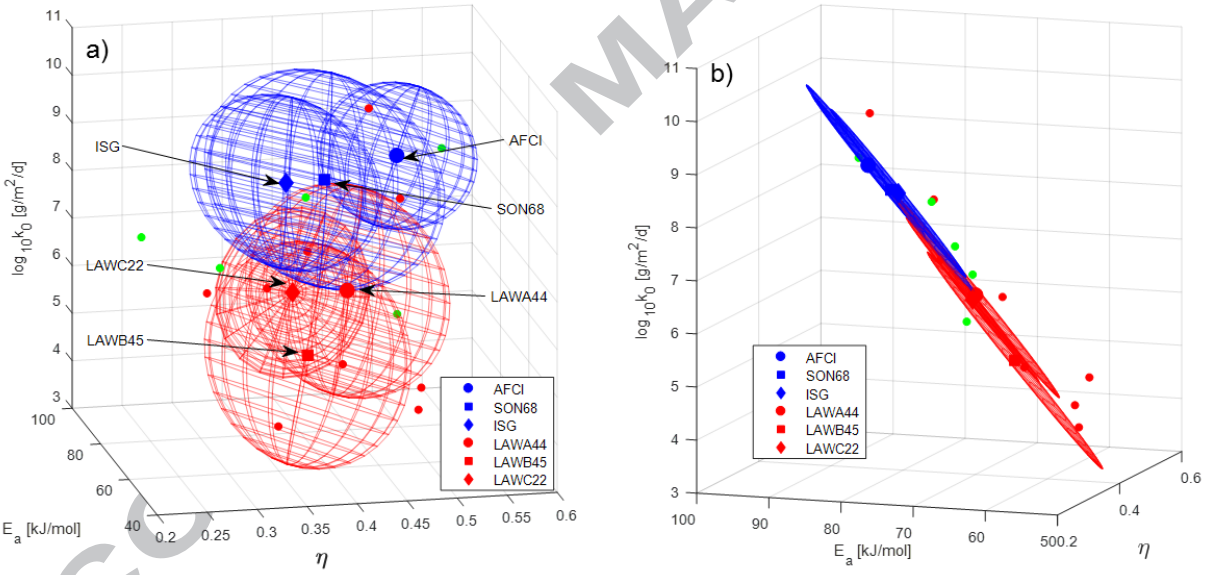

Figure 6a) Plot of mean rate parameter values for AFCI, ISG, SON68 (blue), other HLW glasses (green) and LAW glasses (red) along with ellipses representing the 95% confidence interval for a select number of glasses. b) Same as a) only at another axes rotation. Unlike the ellipsoids, the size of the mean value dots was chosen for visual clarity and not meant to represent any confidence interval.

5. Conclusions

Glasses in contact with aqueous solutions alter and release elements into solution. This exchange of mass between the glass and solution is of interest in several fields; in particular, in the safe storage of nuclear waste

immobilized in borosilicate glasses. In this paper, we present forward rate dissolution data for three simulant borosilicate nuclear waste glasses. Though we note that a more holistic approach to the subject of glass dissolution in a repository environment should include a discussion of the effects of solution species and their effect on the glass dissolution rate, this is not the aim of the present study. Regardless, a study of the forward dissolution rate of glasses in the absence of elevated concentrations of solution species provides a solid basis for the understanding of the mechanism by which glass dissolves in aqueous solutions.

For the three glasses studied here, the forward rate of dissolution is within a factor of 3 despite the different compositions and number of oxides in the different glasses. This suggests that even with this range of glass compositions, the overall reaction controlling the dissolution rate is similar. The data presented in this paper were compared with results from other investigators who studied the same glasses. It was found that rates are similar when the same test method was used, while rates differed when different test methods were used. A system such as the SPFT system that minimizes the effect of pH gradients and the implications of glass fines is an ideal system to measure such rates. This highlights the importance of the test method when determining dissolution rates of different materials as the test method design may result in different rates that are not representative of actual forward dissolution rates of that material.

Lastly, a robust uncertainty analysis was performed for the HLW glasses. The results from this analysis suggest that the model parameters for the rate model of Eq. 3 used to predict glass dissolution behavior in dilute conditions may be highly correlated. This correlation is often overlooked when parameterizing any empirically-based model. Further research will attempt to find a link between glass composition and the rate law parameters. As more glasses are investigated, GCMT will also be expanded to be able to predict the forward rate of glass dissolution based on glass composition.

ACKNOWLEDGMENTS

These studies were supported by the U.S. Department of Energy (DOE) through the Office of Nuclear Energy's Nuclear Technology Research and Development Program. Development of the GCMT model was also supported by Washington River Protection Solutions, Inc. (WRPS) with the support of David Swanberg, Elvie Brown, and Steve Kelly. The authors would like to thank Drs. Sebastien Kerisit (PNNL), John Vienna (PNNL), and Denis Strachan (PNNL) for their technical review of the paper and Kimberly Gray (DOE) for program support. The authors thank

Ian Leavy for ICP-OES technical support and Erin McElroy for assistance in running the tests. Pacific Northwest National Laboratory is operated for the DOE by Battelle Memorial Institute under Contract DE-AC06-76RLO 1830.

6. References

Åagaard P and HC Helgeson (1982) Thermodynamic and kinetic constraints on reaction rates among minerals and aqueous solutions I. Theoretical considerations. *Am. J. Sci.* **282**, 237-285.

Abraitis PK, FR Livens, JE Monteith, JS Small, DP Trivedi, DJ Vaughan and RA Wogelius (2000) The kinetics and mechanisms of simulated British Magnox Waste glass dissolution as a function of pH, silicic acid activity, and time in low temperature aqueous systems. *Appl. Geochem.* **15**, 1399-1416.

Advocat T, JL Crovisier, E Vernaz, G Ehret and H Charpertier (1991) Hydrolysis of R7T7 nuclear waste glass in dilute media: Mechanisms and rate as a function of pH. *Mater. Res. Soc. Symp. Proc.* **212**, 57-64.

Angeli F, T Charpentier, M Gaillard and P Jollivet (2008) Influence of zirconium on the structure of pristine and leached soda-lime borosilicate glasses: Towards a quantitative approach by 17O MQMAS NMR. *J. Non-Cryst. Solids* **354**, 3713-3722.

Bergeron B, L Galoisy, P Jollivet, F Angeli, T Charpentier, G Calas and S Gin (2010) First investigations of the influence of IVB elements (Ti, Zr, and Hf) on the chemical durability of soda-lime borosilicate glasses. *J. Non-Cryst. Solids* **356**, 2315-2322.

Birkholzer J, J Houseworth and C-F Tsang (2012) Geologic Disposal of High-Level Radioactive Waste: Status, Key Issues, and Trends. *Annu. Rev. Environ. Resour.* **37**, 79-106.

Bourcier WL, DW Peiffer, KG Knauss, KD McKeegan and DK Smith (1990) A kinetic model for borosilicate glass dissolution based on the dissolution affinity of a surface layer. *Mater. Res. Soc. Symp. Proc.* **176**, 209-216.

Brantley SL (2008). Kinetics of Mineral Dissolution. Kinetics of Water-Rock Interaction. Eds. (Brantley S. L., Kubicki J. D. and White A. F.), Springer New York**:** 151-210.

Bro R and A Smilde (2014) Principle component analysis. *Analytical Methods* **6**, 2812-2831.

Cailleteau C, F Angeli, F Devreux, S Gin, J Jestin, P Jollivet and O Spalla (2008) Insight into silicate-glass corrosion mechanisms. *Nat. Mater.* **7**, 978-983.

Cantrell KJ, KC Carroll, EC Buck, D Neiner and KN Geiszler (2013) Single-pass flow-through test elucidation of weathering behavior and evaluation of contaminant release models for Hanford tank residual radioactive waste. *Appl. Geochem.* **28**, 119-127.

Cassingham N, C Corkhill, D Backhouse, RJ Hand, JV Ryan, JD Vienna and NC Hyatt (2015) The initial dissolution rates of simulated UK Magnox-ThORP blend nuclear waste glass as a function of pH, temperature adn waste loading. *Mineral. Mag.* **79**, 1529-1542.

Charlton SR and DL Parkhurst (2011) Modules based on the geochemical model PHREEQC for use in scripting and programming languages. *Computers & Geosciences* **37**, 1653-1663.

Criscenti LJ, JD Kubicki and SL Brantley (2006) Silicate glass and mineral dissolution: Calculated reaction paths and activation energies for hydrolysis of a Q^3 Si by $H3O^+$ using ab initio methods. *J. Phys. Chem. A* **110**, 198-206.

Crum JV, AY Billings, JB Lang, JC Marra, CP Rodriguez, JV Ryan and JD Vienna. (2009) Baseline Glass Development for Combined Fission Products Waste Streams: Advanced Fuel Cycle Initiative. AFCI-WAST-WAST-MI-DV-2009-000075, Pacific Northwest National Laboratory, Richland, WA.

Davis LL, JG Darab, M Qian, D Zhao, CS Palenik, H Li, DM Strachan and L Li (2003) Hafnium in peralkaline and peraluminous boro-aluminosilicate glass and glass sub-components: a solubility study. *J. Non-Cryst. Solids* **328**, 102-122.

Delage F and JL Dussossoy (1991) R7T7 glass initial dissolution rate measurements using a high-temperature Soxhlet device. *Mater. Res. Soc. Symp. Proc.* **212**, 41-48.

Doherty J (2015). Calibration and Uncertainty Analysis for Complex Environmental Models. Watermark Numerical Computing, Brisbane, Australia.

Dove PM and DA Crerar (1990) Kinetics of quartz dissolution in electrolyte solutions using a hydrothermal mixed flow reactor. *Geochim. Cosmochim. Acta* **54**, 955-969.

Dove PM (1999) The dissolution kinetics of quartz in aqueous mixed cation solutions. *Geochim. Cosmochim. Acta* **63**, 3715-3727.

Everitt B and H T. (2011). An Introduction to Applied Multivariate Analysis with R. Springer, New York, New York.

Eyring H (1935) The activated complex in chemical reactions. *J. Chem. Phys.* **3**, 107.

Fournier M, S Gin and P Frugier (2014) Resumption of nuclear glass alteration: State of the art. *J. Nucl. Mater.* **448**, 348-363.

Fournier M, A Ull, E Nicoleau, Y Inagaki, M Odorico, P Frugier and S Gin (2016) Glass dissolution rate measurement and calculation revisited. *J. Nucl. Mater.* **476**, 140-154.

Frugier P, S Gin, Y Minet, T Chave, B Bonin, N Godon, JE Lartigue, P Jollivet, A Ayral, L De Windt and G Santarini (2008) SON68 nuclear glass dissolution kinetics: Current state of knowledge and basis of the new GRAAL model. *J. Nucl. Mater.* **380**, 8-21.

Geisler T, T Nagel, MR Kilburn, A Janssen, JP Icenhower, ROC Fonseca, M Grange and AA Nemchin (2015) The mechanism of borosilicate glass corrosion revisited. *Geochim. Cosmochim. Acta* **158**, 112-129.

Gin S, C Guittonneau, N Godon, D Neff, D Rebiscoul, M Cabié and S Mostefaoui (2011) Nuclear Glass Durability: New Insight into Alteration Layer Properties. *J. Phys. Chem. C* **115**, 18696-18706.

Gin S, X Beaudoux, F Angéli, C Jégou and N Godon (2012) Effect of composition on the short-term and long-term dissolution rates of ten borosilicate glasses of increasing complexity from 3 to 30 oxides. *J. Non-Cryst. Solids* **358**, 2559-2570.

Gin S, A Abdelouas, LJ Criscenti, WL Ebert, K Ferrand, T Geisler, MT Harrison, Y Inagaki, S Mitsui, KT Mueller, JC Marra, CG Pantano, EM Pierce, JV Ryan, JM Schofield, CI Steefel and JD Vienna (2013) An international initiative on long-term behavior of high-level nuclear waste glass. *Mater. Today* **16**, 243-248.

Gin S, P Jollivet, M Fournier, F Angeli, P Frugier and T Charpentier (2015) Origin and consequences of silicate glass passivation by surface layers. *Nat. Comm.* **6**, 6360.

Gin S, L Neill, M Fournier, P Frugier, T Ducasse, M Tribet, A Abdelouas, B Parruzot, J Neeway and N Wall (2016) The controversial role of inter-diffusion in glass alteration. *Chem. Geol.* **440**, 115-123.

Grambow B (1985) A general rate equation for nuclear waste glass corrosion. *Mater. Res. Soc. Symp. Proc.* **44**, 15-27.

Gudbrandsson S, D Wolff-Boenisch, SR Gislason and EH Oelkers (2014) Experimental determination of plagioclase dissolution rates as a function of its composition and pH at 22 °C. *Geochim. Cosmochim. Acta* **139**, 154-172.

Guerette M and L Huang (2015) In-situ Raman and Brillouin light scattering study of the international simple glass in response to temperature and pressure. *J. Non-Cryst. Solids* **411**, 101-105.

Hamilton JP, CG Pantano and SL Brantley (2000) Dissolution of albite glass and crystal. *Geochim. Cosmochim. Acta* **64**, 2603-2615.

Hopf J, SN Kerisit, F Angeli, T Charpentier, JP Icenhower, BP McGrail, CF Windisch, SD Burton and EM Pierce (2016) Glass–water interaction: Effect of high-valence cations on glass structure and chemical durability. *Geochim. Cosmochim. Acta* **181**, 54-71.

Icenhower J and PM Dove (2000) The dissolution kinetics of amorphous silica into sodium chloride solutions: Effects of temperature and ionic strength. *Geochim. Cosmochim. Acta* **64**, 4193-4203.

Icenhower JP, A Luttge, BP McGrail, MS Beig, RS Arvidson, EA Rodriguez, JL Steele and SR Baum (2003) Results of vertical Scanning Interferometry (VSI) of dissolved borosilicate glass: Evidence for variable surface features and global surface retreat. *Mater. Res. Soc. Symp. Proc.* **757**, II5.1.

Icenhower JP, BP McGrail, WJ Shaw, EM Pierce, P Nachimuthu, DK Shuh, EA Rodriguez and JL Steele (2008) Experimentally determined dissolution kinetics of Na-rich borosilicate glass at far from equilibrium conditions: Implications for Transition State Theory. *Geochim. Cosmochim. Acta* **72**, 2767-2788.

Icenhower JP and CI Steefel (2013) Experimentally determined dissolution kinetics of SON68 glass at 90 °C over a silica saturation interval: Evidence against a linear rate law. *J. Nucl. Mater.* **439**, 137-147.

Icenhower JP and CI Steefel (2015) Dissolution rate of borosilicate glass SON68: A method of quantification based upon interferometry and implications for experimental and natural weathering rates of glass. *Geochim. Cosmochim. Acta* **157**, 147-163.

Inagaki Y, H Makigaki, K Idemistu, T Arima, S Mitsui and K Noshita (2012) Initial dissolution rate of a Japanese high-level waste glass P0798 as a function of pH and temperature measured by using Micro-Channel Flow-Through test method. *J. Nucl. Sci. Technol.* **49**, 438-449.

Inagaki Y, T Kikunaga, K Idemistu and T Arima (2013) Initial dissolution rate of the International Simple Glass as a function of pH and temperature measured using Microchannel Flow-Through Test method. *Int. J. Appl. Glass Sci.* **4**, 317-327.

Iwalewa TM, T Qu and I Farnan (2017) Investigation of the maximum dissolution rates and temperature dependence of a simulated UK nuclear waste glass in circum-neutral media at 40 and 90°C in a dynamic system. *Appl. Geochem.* **82**, 177-190.

Jegou C, S Gin and F Larche (2000) Alteration kinetics of a simplified nuclear glass in an aqueous medium: effects of solution chemistry and of protective gel properties on diminishing the alteration rate. *J. Nucl. Mater.* **280**, 216-229.

Jeong S-Y and WL Ebert (2002). Glass dissolution rates from static and flow-through tests. Spectrum 2002, Reno, NV, USA, American Nuclear Society.

Jollivet P, S Gin and S Schumacher (2012) Forward dissolution rate of silicate glasses of nuclear interest in clay-equilibrated groundwater. *Chem. Geol.* **330–331**, 207-217.

Knauss KG, WL Bourcier, KD McKeegan, CI Merzbacher, SN Nguyen, FJ Ryerson, DK Smith, HC Weed and L Newton (1990) Dissolution kinetics of a simple nuclear waste glass as a function of pH, time, and temperature. *Mater. Res. Soc. Symp. Proc.* **176**, 371-381.

Köhler SJ, F Dufaud and EH Oelkers (2003) An experimental study of illite dissolution kinetics as a function of pH from 1.4 to 12.4 and temperature from 5 to 50 °C. *Geochim. Cosmochim. Acta* **67**, 3583-3594.

Lasaga AC (1984) Chemical kinetics of water-rock interactions. *J. Geophys. Res.* **89**, 4009-4025.

Lasaga AC (1995). Fundamental approaches in describing mineral dissolution and precipitation rates. Chemical Weathering Rates of Silicate Minerals. Eds. (White A. F. and Brantley S. L.). Washington, DC, Mineralogical Society of America. **31:** 23-86.

McGrail BP, WL Ebert, AJ Bakel and DK Peeler (1997) Measurement of kinetic rate law parameters on a Na-Ca-Al borosilicate glass for low-activity waste. *J. Nucl. Mater.* **249**, 175-189.

McGrail BP, DH Bacon, JP Icenhower, FM Mann, RJ Puigh, HT Schaef and SV Mattigod (2001a) Near-field performance assessment for a low-activity waste glass disposal system: Laboratory testing to modeling results. *J. Nucl. Mater.* **298**, 95-111.

McGrail BP, JP Icenhower, DK Shuh, P Liu, JG Darab, DR Baer, S Thevuthasen, V Shutthanandan, MH Engelhard, CH Booth and P Nachimuthu (2001b) The structure of Na_2O-Al_2O_3-SiO_2 glass: Impact on sodium ion exchange in H_2O and D_2O. *J. Non-Cryst. Solids* **296**, 10-26.

Neeway JJ, A Abdelouas, B Grambow and S Schumacher (2011) Dissolution mechanism of the SON68 reference nuclear waste glass: New data in dynamic system in silica saturation conditions. *J. Nucl. Mater.* **415**, 31-37.

Neeway JJ, SN Kerisit, J Liu, Z J., Z Zhu, B Riley and JV Ryan (2016) Ion-exchange interdiffusion model with potential application to long-term nuclear waste glass performance. *J. Phys. Chem. C* **120**, 9374-9384.

Neeway JJ, RM Asmussen, BP Parruzot, EA Cordova, BD Williams, II Leavy, JR Stephenson and EM McElroy. (2017) FY2016 ILAW Glass Corrosion Testing with the Single-Pass Flow-Through Method. PNNL-26169, RPT-IGPT-013 Rev. 0.0, Pacific Northwest National Laboratory, Richland, WA.

Oelkers EH, J Schott, J-M Gauthier and T Herrero-Roncal (2008) An experimental study of the dissolution mechanism and rates of muscovite. *Geochim. Cosmochim. Acta* **72**, 4948-4961.

Ojovan MI, A Pankov and WE Lee (2006) The ion exchange phase in corrosion of nuclear waste glasses. *J. Nucl. Mater.* **358**, 57-68.

Papathanassiu A, IS Muller, M Brandys, K Gilbo, A Barkatt, I Joseph and IL Pegg. (2011) ILAW Glass Testing for Disposal at IDF: Phase 1 Testing. VSL-11R2270-1, Vitreous State Laboratory, The Catholic University of America, Washington, DC.

Pederson LR, DR Baer, GL McVay and MH Engelhard (1986) Reaction of soda lime silicate glass in isotopically labelled water. *J. Non-Cryst. Solids* **86**, 369-380.

Pierce EM, BP McGrail, EA Rodriguez, HT Schaef, KP Saripalli, RJ Serne, PF Martin, SR Baum, KN Geizler, LR Reed and WJ Shaw. (2004) Waste Form Release Data Package for the 2005 Integrated Disposal Facility Performance Assessment. PNNL-14805, Pacific Northwest National Laboratory, Richland, WA.

Pierce EM, EA Rodriguez, LJ Calligan, WJ Shaw and BP McGrail (2008) An experimental study of the dissolution rates of simulated aluminoborosilicate waste glasses as a function of pH and temperature under dilute conditions. *Appl. Geochem.* **23**, 2559-2573.

Pierce EM, LR Reed, WJ Shaw, BP McGrail, JP Icenhower, CF Windisch, EA Cordova and J Broady (2010) Experimental determination of the effect of the ratio of B/Al on glass dissolution along the nepheline ($NaAlSiO_4$)-malinkoite ($NaBSiO_4$) join. *Geochim. Cosmochim. Acta* **74**, 2634-2654.

Pollyea RM and JD Rimstidt (2017) Rate equations for modeling carbon dioxide sequestration in basalt. *Appl. Geochem.* **81**, 53-62.

Rieke PC and SN Kerisit. (2016) Modeling Tool Enhancement. PNNL-25111, Pacific Northwest National Laboratory, Richland, WA.

Rimstidt JD and HL Barnes (1980) The kinetics of silica-water reactions. *Geochim. Cosmochim. Acta* **44**, 1683-1699.

Schaef HT and BP McGrail (2009) Dissolution of Columbia River Basalt under mildly acidic conditions as a function of temperature: Experimental results relevant to the geological sequestration of carbon dioxide. *Appl. Geochem.* **24**, 980-987.

Shutthanandan V, DR Baer, S Thevuthasan, EM Adams, S Maheswaran, MH Engelhard, JP Icenhower and BP McGrail (2002) High energy ion beam studies of ion exchange in a Na_2O-Al_2O_3-SiO_2 glass. *J. Appl. Phys.* **91**, 1910-1920.

Strachan D (2017) Glass dissolution asa function of pH and its implications for understanding mechanisms and future experiments. *Geochim. Cosmochim. Acta* **219**, 111-123.

Strachan DM and TL Croak (2000) Compositional effects on long-term dissolution of borosilicate glass. *J. Non-Cryst. Solids* **272**, 22-33.

Strachan DM (2001) Glass dissolution: testing and modeling for long-term behavior. *J. Nucl. Mater.* **298**, 69-77.

Strachan DM and JJ Neeway (2014) Effects of alteration product precipitation on glass dissolution. *Appl. Geochem.* **45**, 144-157.

Tournié A, O Majérus, G Lefèvre, MN Rager, S Walmé, D Caurant and P Barboux (2013) Impact of boron complexation by Tris buffer on the initial dissolution rate of borosilicate glasses. *J. Colloid Interface Sci.* **400**, 161-167.

Van Iseghem P and B Grambow (1988) The long-term corrosion and modelling of two simulated Belgian reference high-level waste glasses. *Mater. Res. Soc. Symp. Proc.* **112**, 631-639.

Van Iseghem P, M Aerstens, S Gin, D Deneele, B Grambow, DM Strachan, BP McGrail and GG Wicks (2009). GLAMOR - Or how we achieved a common understanding on the decrease of glass dissolution kinetics. Ceramic Transactions, Westerville, OH, American Ceramic Society.

Wolery TJ. (1992) EQ3NR, A Computer Code for Geochemical Aqueous Speciation-Solubility Calculations: Theoretical Manual, Users' Guide and Related Documentation (Version 7.0). UCRL-MA-110662 PT 1, Lawrence Livermore National Laboratory, Livermore, CA.

Wolff-Boenisch D, SR Gislason, EH Oelkers and CV Putnis (2004) The dissolution rates of natural glasses as a function of their composition at pH 4 and 10.6, and temperatures from 25 to 74°C. *Geochim. Cosmochim. Acta* **68**, 4843-4858.

Zapol P, H He, KD Kwon and LJ Criscenti (2013) First-principles study of hydrolysis reaction barriers in a sodium borosilicate glass. *Int. J. Appl. Glass Sci.* **4**, 395-407.

Table of Contents/Abstract Graphic